Met. Mater. Int., Vol. 21, No. 4 (2015), pp. 673~677
doi: 10.1007/s12540-015-4580-x

Porosity Effects of a Fe-Based Amorphous/Nanocrystals Coating Prepared by a Commercial High Velocity Oxy-Fuel Process on Cavitation Erosion Behaviors

Y. J. Kim[1], J. W. Jang[2], D. W. Lee[2], and S. Yi[1,*]

[1]Department of Materials Science and Metallurgical Engineering, Kyungpook National University, Daehak-ro 80, Daegu 702-701, Korea
[2]STX Heavy Industry Company, Dalsu-gu Dalsudae-ro 633, Daegu 704-946, Korea

(received date: 27 Novemner 2014 / accepted date: 6 March 2015)

Coatings with different porosities were prepared by controlling high velocity oxy-fuel process parameters. Pores were distributed homogeneously along the thickness of the coatings. Cavitation erosion rate of the coating was obtained by a vibratory cavitation equipment following ASTM G32 standard. As porosity of the coating increases, the cavitation erosion rate increases. Significantly high cavitation erosion rate was obtained in the early stage of the test for the coating with high porosity. As cavitation erosion test proceeds, the cavitation erosion rate tends to decrease. Cracks initiated in the surface pore area propagate along powder boundaries and merge to pores near surface. Due to the cracks, large coating parts consisting of a bunch of powders with good bonding were detached from the coating increasing the cavitation erosion rate. Corrosion products were preferentially formed on the pore areas enhancing the cavitation erosion rate. Consequently, pores near coating surface significantly accelerate the cavitation erosion rate through mechanical as well as chemical manners.

Keywords: plasma deposition/spray, erosion, amorphous materials, corrosion, nanostructured materials

1. INTRODUCTION

Cavitation erosion management of ship propellers has been a critical factor for the improvement of fuel efficiency and the repair period of a ship [1-3]. For the cavitation erosion mechanism, there have been many discussions regarding hydrodynamic as well as material aspects [4-6]. However, since the cavitation erosion occurs through complex phenomena, a clear explanation of cavitation erosion has not been made to date. Moreover, ship propellers are exposed to a sea water containing high concentrations of chloride ion (Cl^-) and solid particles and thus, corrosive erosion rate can be significantly accelerated in comparison with the erosion rate within a clean water.

From the view point of material properties, high strength and toughness as well as high corrosion resistance in a sea water are needed to enhance cavitation erosion resistance. Therefore, several kinds of ceramic coatings have been applied to improve cavitation erosion resistance through various coating processes. Also, some alloys such as stainless steels or Ti alloys have been coated on the propeller with the same purpose [7,8]. When the coating process is applied for cavitation erosion protection, surface roughness and porosity of the coating should be controlled to minimum levels.

*Corresponding author: yish@knu.ac.kr

Recently, Fe-based bulk metallic glasses or nanocomposites with an amorphous matrix have been considered as potential materials for anti-corrosive erosion applications [9-13]. Amorphous phase yields beneficial properties (strength, resilience and corrosion resistance) attributed to unique atomic arrangement without any crystallographic defects [14]. Besides, some Fe-based bulk metallic glasses with high glass forming ability can be cost-effectively coated through commercial coating processes including various thermal spray coating processes [9,15]. In this study, a Fe-based bulk metallic glass was coated on a Cu alloy substrate by a commercial high velocity oxy-fuel (HVOF) process. By changing the HVOF process parameters, three coatings with identical composition but different microstructures were prepared to investigate effects of porosity of the coating on cavitation erosion properties. The cavitation erosion test was conducted in a vibratory cavitation equipment following ASTM G32 standard and the results were discussed on the basis of microstructural analysis of the coating.

2. EXPERIMENTAL PROCEDURE

Coatings with the nominal composition of $Fe_{64}Si_{3.5}B_{3.5}Cr_{15}Mo_1Nb_6$ were prepared by a commercial HVOF process on the Cu based alloy substrate having the chemical composition listed in Table 1. Gas atomized powders with the size of around 40 μm were used for the HVOF process. To control

Table 1. Chemical compositions of atomized powders and the substrate (wt%)

	Fe	Si	B	Cr	Mo	Ni	Mn	Nb	Cu	Pb	Sn	Al	Zn	Mn
Atomize powder (nominal comp.)	64.000	3.500	15.000	1.000	6.000	1.000	6.000	-	-	-	-	-	-	-
Substrate (ALBC3)	3.000 ~6.000	-	-	-	-	3.000 ~6.000	-	-	78.000 ~85.000	<0.1	<0.100	8.500 ~10.500	<0.500	0.100 ~1.500

Table 2. HVOF process parameters for the coatings with different porosities

	Combustion Pressure [psi]	Working distance [mm]	Gun rate [mm/ses]	Powder feed disc rotate speed [rpm]	Oxygen/Fuel (Kerosene) [psi]
Porosity (3.6)	70	300	200	6	140/120
Porosity (1.4)	80	330	200	6	105/97
Porosity (0.6)	85	380	200	6	111/103

porosity of the coating, HVOF parameters were varied as summarized in Table 2. Microstructures of the coatings were analyzed using an optical microscopy and a scanning electron microscopy (SEM, HITACHI 4300 SEM, 15 KV), and X-ray diffractometry (XRD, Philips X'Pert diffractometer) with Cu radiation (Cu-Kα, λ=0.1541 nm). Porosities of the coatings were measured from optical images of cross sections of the coatings using an image analysis program. Porosity measurements were performed at high magnification (X500) using an image analyzer (i-Solution Delta/IMT). Four different regions for each sample were measured and the average value for the measurements was obtained for each sample. Micro hardness was measured using HM-112/(Mitutoyo) Vickers hardness tester under the load of 100 g. Thermal properties of coatings were analyzed with a differential scanning calorimeter (DSC, Pyris Diamond DSC) at a heating rate of 10 K/min. Cavitation erosion resistances of the coatings were estimated using a vibratory cavitation equipment following ASTM G32 standard as schematically illustrated in Fig. 1. Ultrasonic vibrator (SEE-SONIN2/ULTECH) with the frequency of 20 kHz was used in a distilled water at 25 ± 0.1 ℃. The sample was located 12 mm below the water surface. After cavitation erosion test for a desired period, the sample was cleaned with ethanol using an ultrasonic cleaner and then, dried with hot air. The weight changes after tests were measured by an electronic balance with the accuracy of 0.1 mg. Corrosion behaviors of coatings with different porosities were investigated through immersion tests in a 3.0 wt% NaCl solution.

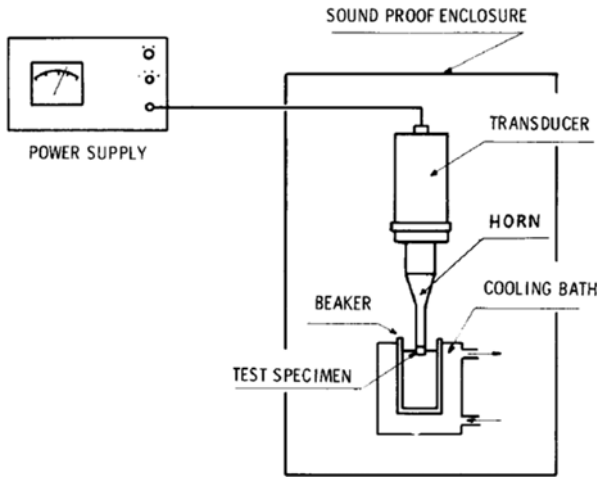

Fig. 1. Schematic illustration of the vibratory cavitation equipment.

3. RESULTS AND DISCUSSION

3.1. Microstructures of the coatings

Optical micrographs of coatings prepared by three coating conditions listed in Table 2 were shown in Fig. 2, respectively. Coatings with the thickness of around 400~500 μm formed on the Cu alloy substrates with good bonding strengths (>30N/mm^2). Porosities in the range of 0.56~3.60 were measured from the cross section images. The XRD result for the coating exhibits sharp peaks for crystalline phases along with a halo pattern typical for amorphous phase (Fig. 3). Although the cooling rate of HVOF process is high enough to form fully amorphous

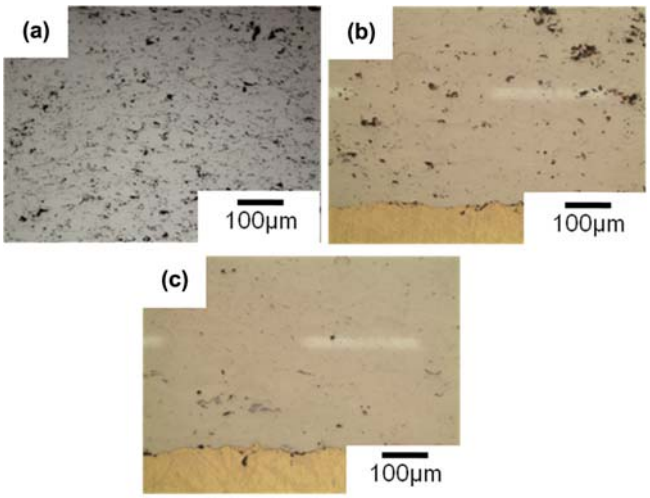

Fig. 2. Optical micrographs of cross sections of coatings formed with different porosities of 3.6 ± 0.6 (a), 1.4 ± 0.4 (b), and 0.6 ± 0.2 (c) respectively.

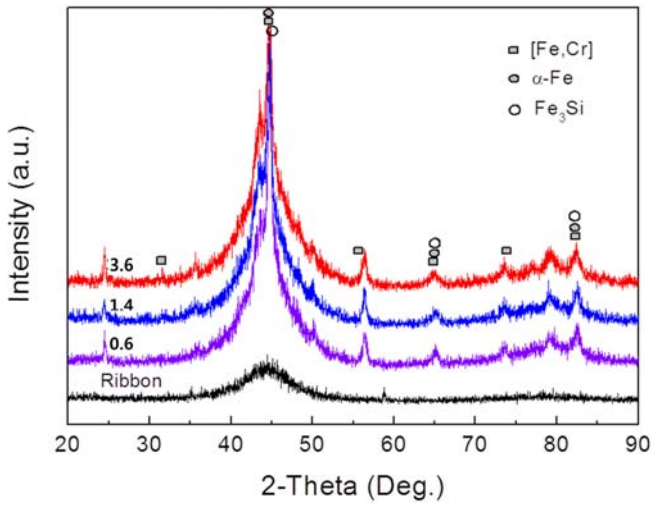

Fig. 3. XRD results for the coating and the melt-spun ribbon, respectively.

coating of the Fe-based amorphous alloy, partial crystallization can occur after deposition of liquid droplets. That is, even after deposition, liquid droplets continuously deposit on the pre-deposited layer raising the pre-deposited layer temperature causing partial crystallization of the pre-deposit layer. As a result, coatings with nanocrystalline phases embedded within an amorphous matrix were prepared through the HVOF coating process conditions applied in this study.

DSC heating curve of the coating exhibited three crystallization peaks as in the case of melt-spun ribbon that is fully amorphous phase. However, the amount of heat released during the phase transformation of amorphous phase to crystalline phases in the coating was smaller than that in the ribbon indicating partial crystallization during HVOF coating process occurred to some extent (Fig. 4). Therefore, it is inferred from

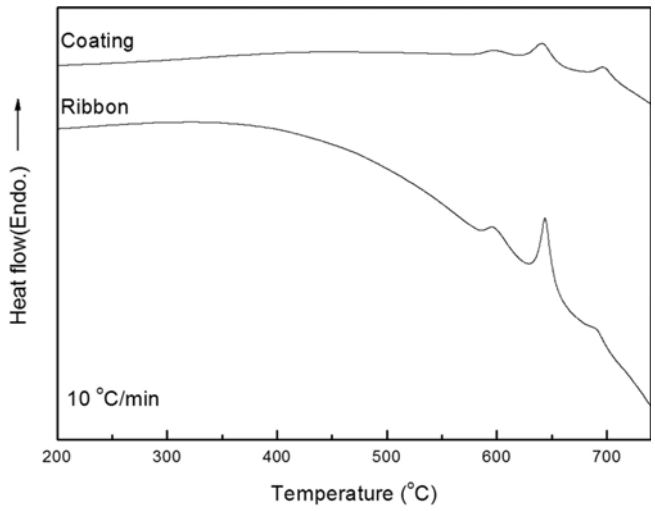

Fig. 4. DSC results for the coating and the as-melt spun ribbon, respectively.

the XRD and DSC results that partial crystallization occurred during the coating process.

As the porosity of coating decreases, the average microhardness value of coating tends to decrease. The average microhardness values (Hv) of 690, 786 and 828 Hv were obtained for the coatings with porosities of 3.6 ± 0.6, 1.4 ± 0.4 and 0.6 ± 0.2, respectively. Also, the micorhardness value of 201 Hv was obtained for the Cu alloy substrate.

3.2. Cavitation erosion test results

Weight losses during cavitation erosion tests were measured every hour as shown in Fig. 5. The weight losses of coatings with the porosity of 0.6 ± 0.2 and 1.4 ± 0.4 were much lower than that of the coating with the porosity of 3.6 ± 0.6. In general, cavitation erosion rate decreases as the hardness of coated materials increases. Since the atomized powders made of the same batch of melt were used for the coatings, mechanical properties of coated powders were not significantly changed by coating process parameters. Therefore, the difference

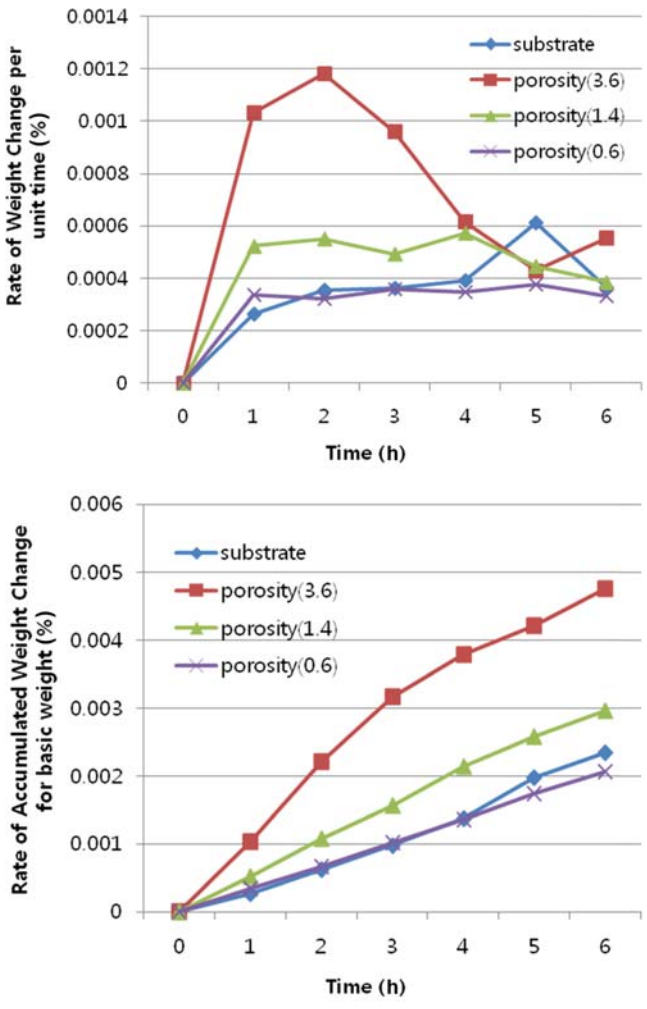

Fig. 5. Results of cavitation erosion tests following ASTM G35 standard in a distilled water.

in cavitation erosion rate was attributed to microstructural aspects of the coatings. Among coatings, it can be known from Fig. 5 that the cavitation erosion resistance of coating tends to increase as microhardness value of the coating increases. However, the cavitation erosion rate of Cu alloy substrate with much low hardness was higher than those of the coatings during the test for about 1 hour. It should be noted that initial cavitation erosion rates of the coating with the porosity of 3.6 ± 0.6 were significantly higher than latter cavitation erosion rates. In the early period of the cavitation erosion test, i.e., the test for up to 3 hours, significant weight loss of the coating with high porosity of 3.6 ± 0.6 occurred, while relatively low weight losses with constant rates occurred in the coatings with low porosities of 0.6 ± 0.2 and 1.4 ± 0.4. High weight loss can be attributed to the high porosity in the early stage of the test. Bubble formation can be enhanced near pores and thus, severe micro-jet and/or shock wave can be preferentially impacted near the pore areas. During enhanced impaction near pore areas,

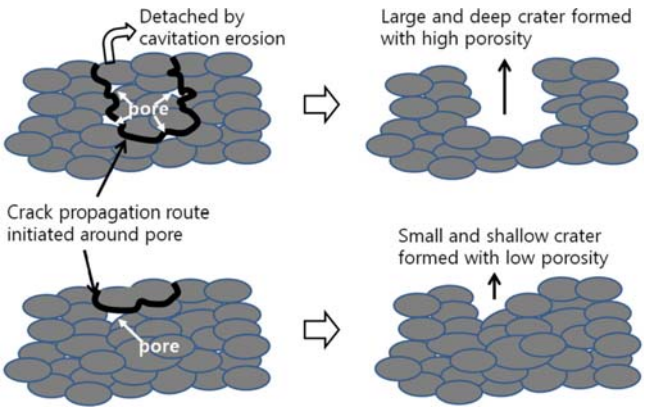

Fig. 6. Schematic illustrations for failure modes of HVOF-sparyed coatings with high and low porosity, respectively.

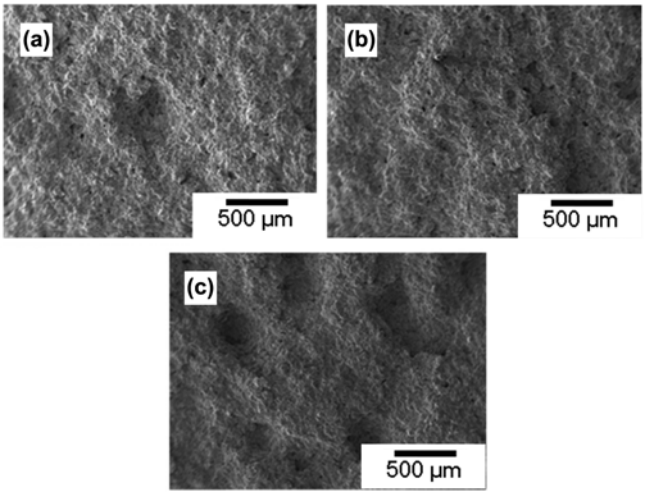

Fig. 7. SEM images of surface morphologies of the samples with different porosities ((a) 0.6 ± 0.2, (b) 1.4 ± 0.4, and (c) 3.6 ± 0.6) after cavitation erosion tests.

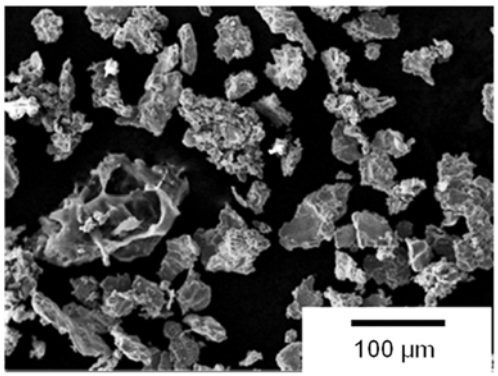

Fig. 8. Morphologies of detached coating parts after the cavitation test for 2 hours.

stress concentration occurs between powder boundaries leading to detachment of coated powder layers [6,8]. In the coating with high porosity, cracks that were initiated around pore areas propagate along the powder boundaries. The cracks and pores beneath the surface merge together leading to the detachment of large amounts of coating materials as schematically explained in Fig. 6. As cavitation erosion proceeds, number of pores contributing to the detachment of large coating parts decreases and thus, cavitation erosion rate tends to decrease as can be inferred from Fig. 5. That is, pores far from the surface of coating would not significantly affect the cavitation erosion rate.

Figure 7 shows the surface morphologies of the coatings after cavitation erosion tests. As can be expected from the above discussion, relatively large and deep cavities were formed in the coating with the porosity of 3.6 ± 0.6. Figure 8 shows the morphologies of collected residues after the cavitation test for 2 hours. Large and long residues including many coated particles with good bonding were collected demonstrating the detachment mechanism of the coating material with high porosity.

3.3. Corrosion behaviors of the coatings within a 3.0 wt% NaCl solution

Figure 9 shows the surfaces of the coatings after immersion tests for 4 hours. The corrosion area tends to increase as the porosity. Since surface pore areas can act as nucleation sites

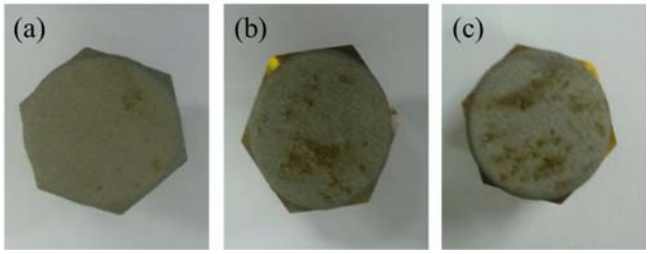

Fig. 9. Optical micrographs of the coating surfaces after the immersion tests in a 3.0 wt% NaCl solution for 4 h. Porosity of (a) 3.6±0.6, (b) 1.4±0.4, and (c) 0.6±0.2, respectively.

for corrosion products, the corrosion area increases with the increase of porosity.

4. CONCLUSION

Coatings with nanocrystals embedded in the Fe-based amorphous matrix were prepared through a commercial HVOF process using atomized powders with the nominal composition of $Fe_{64}Si_{3.5}B_{3.5}Cr_{15}Mo_1Nb_6$. By controlling HVOF process parameters, coatings with the porosities of 0.6 ± 0.2, 1.4 ± 0.4 and 3.6 ± 0.6, respectively, were prepared to study porosity effects on the cavitation erosion. In the early stage of cavitation erosion test for the coating with the porosity of 3.6 ± 0.6, high cavitation erosion rate was observed while relatively low cavitation erosion rate was obtained in the latter stage. Pores near the coating surface act as nucleation sites for bubble formation and thus, preferential sites for micro-jet impaction. Cracks initiated by stress concentration in the pore area propagate along powder boundaries and merged into pores beneath the surface leading to the detachment of large coating parts consisting of powders with good bonding. Also, pores on the surface act as nucleation sites for corrosion product formation in a 3.0 wt% NaCl water. Therefore, it is concluded that pores near surface significantly enhance the cavitation erosion rate as well as corrosion rate of the coating.

ACKNOWLEDGMENT

This work was supported by Korea Institute of Energy Technology Evaluation (Project No. 2012T100100377).

REFERENCES

1. R. B. Rebak, S. D. Day, T. Lian, P. D. Hailey, and J. C. Farmer, *the Minerals, Metals & Materials Society* **39**A, 225 (2008).
2. M. Telford, *Materials Today* **7**, 36 (2004).
3. X. Y. Li, Y. G. Yan, L. Ma, Z. M. Xu, and J. G. Li, *Mater. Sci. and Eng. A* **382**, 82 (2004).
4. J. F. Santa, L. A. Espitia, J. A. Blanco, S. A. Romo, and A. Toro, *Wear*, **267**, 160 (2009).
5. D. Carnelli, A. Karimi, and J. PierreFranc, *Wear*, **289**, 104 (2012).
6. J. Lin, Z. Wang, P. Lin, J. Cheng, X. Zhang, and S. Hong, *Surf. Coat. Technol.* **240**, 432 (2014).
7. H. Mochizuki, M. Yokota, and S. Hattori, Wear, **262**, 522 (2007).
8. G. Hou, X. Zhao, H. Zhou, J. Lu, Y. An, J. Chen, and J. Yang, *Wear*, **311**, 81 (2014).
9. B. T. Jang, S. S. Kim, and S. Yi, *Met. Mater. Int*. **20**, 55 (2014).
10. W. Yuping, L. Pinghua, C. Chenglin, W. Zehua, C. Ming, and H. Junhua, *Materials Letters*, **61**, 1867 (2007).
11. Z. B. Zheng, Y. G. Zheng, W. H. Sun, and J. Q. Wang, *Corros. Sci.* **76**, 337 (2013).
12. S. L.Wang, H. X. Li, X. F. Zhanga, and S. Yi, *Mater. Chem. Phys*. **113**, 878 (2009).
13. S. L. Wang, H. X. Li, S. Y. Hwang, S. D. Choi, and S. Yi, *Met. Mater. Int.* **18**, 607 (2012).
14. S. J. Pang, T. Zhang, K. Asami, and A. Inoue, *Corros. Sci.* **44**, 1847 (2002).
15. S. M. Jung, J. H. Do, D.-G. Lee, B.-J. Lee, G.-U. Cha, and S. H. Lee, *Met. Mater. Int*. **20**, 577 (2014).